Monthly Notices
of the
ROYAL ASTRONOMICAL SOCIETY

MNRAS **489,** 3648–3654 (2019)
Advance Access publication 2019 August 29

doi:10.1093/mnras/stz2394

A magnetic white dwarf with five H α components

Mukremin Kilic [1]★ B. Rolland,[2] P. Bergeron,[2] Z. Vanderbosch,[3,4] P. Benni[5] and J. Garlitz[6]

[1]*Homer L. Dodge Department of Physics and Astronomy, University of Oklahoma, 440 W. Brooks St., Norman, OK 73019, USA*
[2]*Département de Physique, Université de Montréal, C.P. 6128, Succ. Centre-Ville, Montréal, QC H3C 3J7, Canada*
[3]*Department of Astronomy, University of Texas at Austin, Austin, TX 78712, USA*
[4]*McDonald Observatory, Fort Davis, TX 79734, USA*
[5]*Acton Sky Portal, 3 Concetta Circle, Acton, MA 01720, USA*
[6]*Private Observatory, 1155 Hartford St., Elgin, OR 97827, USA*

Accepted 2019 August 28. Received 2019 August 19; in original form 2019 June 28

ABSTRACT

G183−35 is an unusual white dwarf that shows an H α line split into five components, instead of the usual three components seen in strongly magnetic white dwarfs. Potential explanations for the unusual set of lines include a double degenerate system containing two magnetic white dwarfs and/or rotational modulation of a complex magnetic field structure. Here, we present time-resolved spectroscopy of G183−35 obtained at the Gemini Observatory. These data reveal two sets of absorption lines that appear and disappear over a period of about 4 h. We also detect low-level (0.2 per cent) variability in optical photometry at the same period. We demonstrate that the spectroscopic and photometric variability can be explained by the presence of spots on the surface of the white dwarf and a change in the average field strength from about 4.6 to 6.2 MG. The observed variability is clearly due to G183−35's relatively short spin period. However, rotational modulation of a complex magnetic field by itself cannot explain the changes seen in the central H α component. An additional source of variability in the line profiles, most likely due to a chemically inhomogeneous surface composition, is also needed. We propose further observations of similar objects to test this scenario.

Key words: magnetic fields – stars: evolution – stars: individual: G183−35, NLTT 46206, WD 1814+248 – stars: rotation – starspots – white dwarfs.

1 INTRODUCTION

About 10–20 per cent of white dwarfs in the solar neighbourhood are strongly magnetic, with field strengths of up to 10^9 G (Kawka et al. 2007; Brinkworth et al. 2013; Ferrario, de Martino & Gänsicke 2015). Weak fields, $B \leq 1$ kG, may also be present in most white dwarfs, but are hard to detect (Jordan et al. 2007; Landstreet et al. 2012). Magnetic white dwarfs tend to be on average higher in mass compared to their non-magnetic counterparts (Liebert 1988; Kawka et al. 2007; Briggs et al. 2015). Curiously, high-field magnetic white dwarfs are never found in wide binary systems with late-type stellar companions (Liebert et al. 2005). This led to Tout et al. (2008) and Briggs et al. (2015, 2018) to suggest that merging binaries within a common envelope can explain the incidence of magnetism and the mass distribution of high-field magnetic white dwarfs.

Several high-field magnetic white dwarfs are confirmed to be in common proper motion or short-period binaries with other white dwarfs (Ferrario et al. 1997; Girven et al. 2010; Dobbie et al. 2012). For example, NLTT 12758 is a magnetic white dwarf with a non-magnetic companion white dwarf in a 1.154 d orbit (Kawka et al. 2017). Rolland & Bergeron (2015) analysed 16 magnetic DA white dwarfs with high signal-to-noise ratio optical spectroscopy available and found that offset dipole models can explain six of these stars. However, the remaining 10 stars in their sample have photometric temperatures that are inconsistent with their spectroscopy, and these may be in unresolved binary systems. However, the overabundance of binary candidates in such a small sample of high-field magnetic white dwarfs is intriguing. One of these stars, G183−35 (also known as NLTT 46206 and WD 1814+248) displays an H α line that is split into five components, which could be due to a combination of two magnetic DA white dwarfs in this system (Rolland & Bergeron 2015).

G183−35 was identified as a high proper motion object by Giclas, Burnham & Thomas (1971) and classified to be a DC white dwarf by Hintzen & Strittmatter (1974) based on low-resolution spectroscopy. Putney (1995) performed a spectropolarimetric survey of several white dwarfs, including G183−35, and detected that H lines split into three components due to a magnetic field strength of 6.8 ± 0.5 MG. In addition, she found evidence of a change in both

★ E-mail: kilic@ou.edu

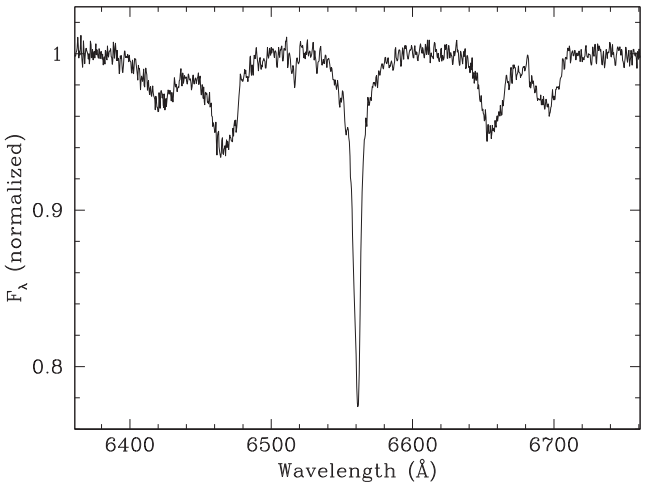

Figure 1. The average spectrum of G183−35 based on our Gemini data. This spectrum has a signal-to-noise ratio of 250 in the continuum and reveals a central Hα line along with two other sets of Zeeman-split lines that are separated from the central component by about 95 and 140 Å, respectively. Note that the weak absorption feature near 6516 Å is telluric.

line shapes and polarization spectra taken more than a year apart and interpreted this as evidence of rotation in this object. To search for a rotation period, Brinkworth et al. (2013) obtained follow-up photometry of G183−35, but did not find any evidence of variability at the ≥4 per cent level on time-scales of less than a year.

To explore the origin of the unusual splitting of the Hα line in G183−35, we obtained time-resolved spectroscopy and photometry over multiple nights. Here we present the results of this study. We list the details of our observations in Section 2, discuss the variability in the line shapes, radial velocity of the central Hα line, and photometry in Section 3. We constrain the physical parameters of G183−35, including its rotation period, in Section 4, and conclude in Section 5.

2 OBSERVATIONS

We obtained follow-up optical spectroscopy of G183−35 using the 8 m Gemini North telescope equipped with the Gemini Multi-Object Spectrograph (GMOS) as part of the Fast Turnaround queue programme GN-2017B-FT-2. We obtained a sequence of 32 × 5 min long back-to-back exposures on UT 2017 September 10 with the R831 grating and a 0.5 arcsec slit, providing wavelength coverage from 5350 to 7710 Å and a resolution of 0.376 Å per pixel. Each spectrum has a comparison lamp exposure taken within 10 min of the observation time. We obtained additional sets of 4 and 10 back-to-back exposures on UT 2017 September 11 and 12, respectively. We used the IRAF GEMINI GMOS package to reduce these data. Fig. 1 shows our summed Gemini spectrum based on 46 exposures. This spectrum has a signal-to-noise ratio of 250 in the continuum, and clearly shows a narrow central Hα line, and four other Zeeman-split Hα lines as noted by Rolland & Bergeron (2015).

We obtained follow-up *V*-band optical photometry of G183−35 with 1 min long exposures over 5.9 h on UT 2017 June 15 using a 35 cm Schmidt-Cassegrain telescope at the Acton Sky Portal in Massachusetts. We also obtained white-light optical photometry of the same target with 6 min long exposures over 5.5 h on UT 2017 June 22 using a Celestron 28 cm telescope at a private observatory in Oregon.

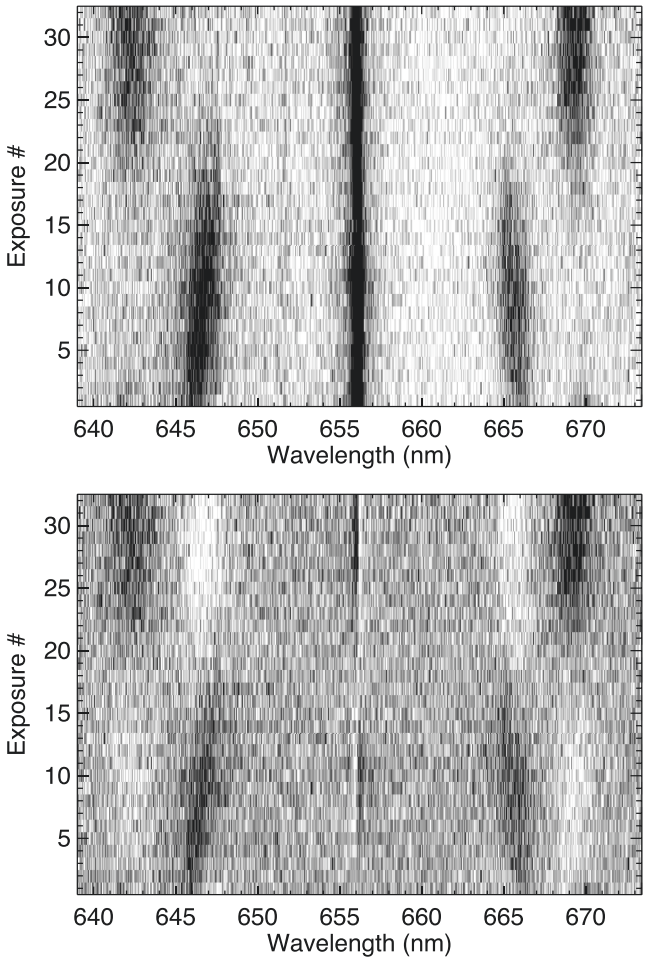

Figure 2. *Top:* Gemini time-resolved spectroscopy of G183−35 over 2.9 h on UT 2017 September 10. *Bottom:* The difference image between each spectrum shown above and the average spectrum.

We obtained additional follow-up time-series photometry on UT 2017 June 21–25 and July 26–29 using the McDonald Observatory 2.1 m Otto Struve telescope with the ProEM camera and the BG40 filter. We used exposure times of 10–30 s with a total integration time of 19.88 h. We binned the CCD by 4 × 4, which resulted in a plate scale of 0.38 arcsec pixel^{-1}. We used several comparison stars to correct for transparency variations.

3 RESULTS

3.1 Spectroscopic variability

Fig. 2 shows the Gemini/GMOS trailed spectrum of G183−35 based on 32 back-to-back exposures taken over 2.9 h on UT 2017 September 10. This figure reveals relatively quick changes in the line profiles. The central Hα component is always there, but the other components, the inner and outer sets of lines appear and disappear in sequence. The first exposure has both sets of lines visible (the inner and outer pairs), but then only the inner pair is visible with a separation of ≈100 Å from the central component. The inner pair stays visible for about 20 exposures (each exposure is 5 min long), but its separation from the central component decreases over time to ≈90 Å. At this point, the inner pair of lines disappears, and the wider pair of lines becomes visible. The wider pair remains at about

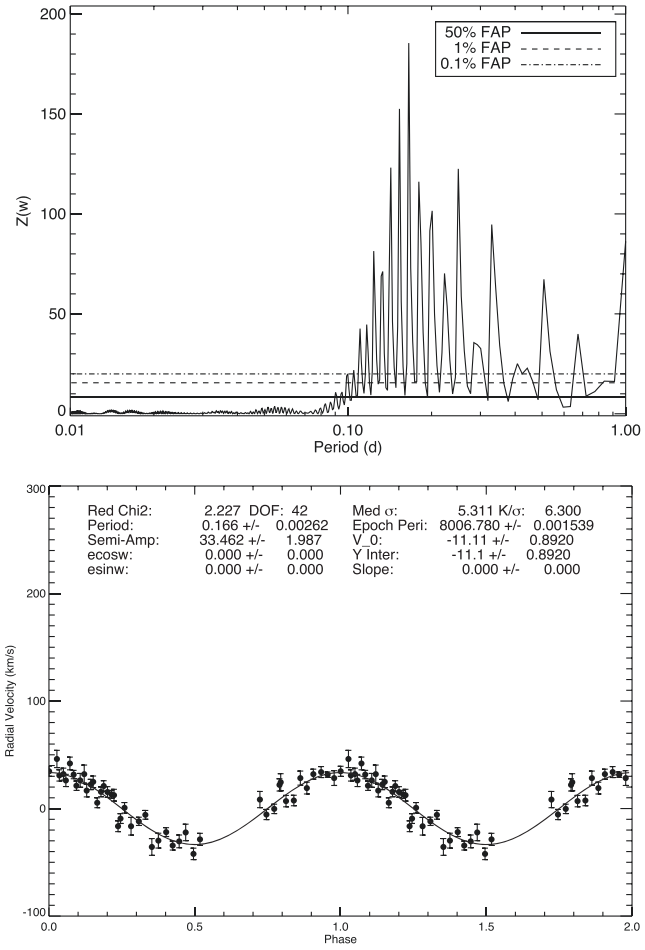

Figure 3. *Top:* Lomb–Scargle periodogram of the radial velocity of the central H α component. The solid, dashed, and dashed-dotted lines mark the 50, 1, and 0.1 per cent false-alarm probability limits. *Bottom:* The best-fitting solution assuming a circular orbit.

the same wavelength for the rest of the observations on the same night.

We have an additional set of 14 spectra taken on consecutive nights (not shown here). These spectra also display the change in the inner pair of lines over short time-scales. We measured the equivalent widths of the inner and outer pairs of lines in each spectrum, and found three significant peaks at 0.142, 0.153, and 0.166 d in a Lomb–Scargle diagram (Lomb 1976; Scargle 1982) of these equivalent width measurements.

The bottom panel in Fig. 2 shows the differences between the trailed spectrum of G183−35 (shown in the top panel) and its average spectrum. The shift in wavelength of the inner pair of lines compared to the average spectrum is clearly visible. The missing absorption features in each spectrum (compared to the average) appear brighter. More importantly, this figure also reveals a significant shift in the wavelength of the central H α line over time. To verify that this shift in the central component is not due to the spectrograph flexure, we used the telluric lines between 7160 and 7400 Å in each Gemini spectrum. We measured an average velocity offset of $-0.2 \pm 2.5\,\mathrm{km\,s^{-1}}$ in this wavelength range. Hence, the systematic errors in our radial velocity measurements are of the order of only a few $\mathrm{km\,s^{-1}}$.

We used the cross-correlation package RVSAO (Kurtz & Mink 1998) to measure the radial velocity of the H α line in the wavelength

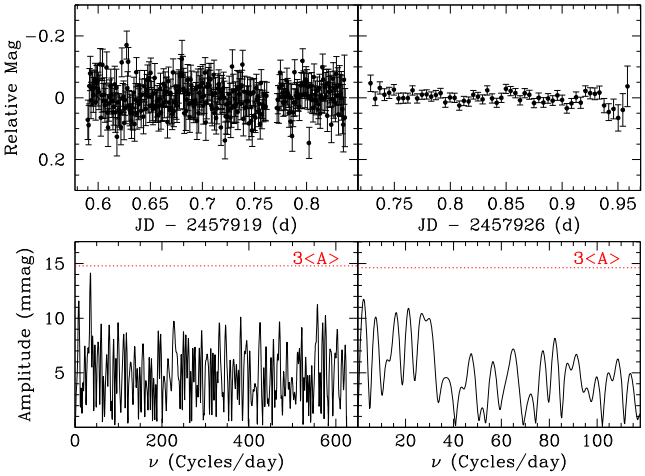

Figure 4. Time-series photometry of G183−35 obtained over 5.9 and 5.5 h at Acton Sky Portal (top left) and a private observatory in Oregon (top right) on two different nights in 2017 June. The bottom panels show the Fourier transform and the 3 $<A>$ detection limit for each data set, where $<A>$ is the average amplitude in the frequency range shown.

range 6500−6620 Å. We used the average spectrum of G183−35 as the template spectrum, since we are only interested in constraining the relative shifts in the central H α line. Our final velocities come from cross-correlating the individual observations with this template.

To search for periodicities in the radial velocity data, we computed the Lomb–Scargle periodogram using the IDL program MPRVFIT (De Lee et al. 2013). Fig. 3 shows the Lomb–Scargle periodogram and the best-fitting solution assuming a circular orbit. The highest peak is at $P = 0.166$ d, which implies a velocity semi-amplitude of $K = 33.5 \pm 2.0\,\mathrm{km\,s^{-1}}$ and a mass function of $f = 0.00064 \pm 0.00011\,\mathrm{M_\odot}$. However, just like in the equivalent width measurements of the inner and outer pairs of lines discussed above, there are several significant aliases in the periodogram, including 0.142 and 0.153 d. Note that these frequencies are separated from each other by the daily alias (11.57 μHz), which makes it hard to identify the exact frequency of variation.

3.2 Photometric variability

Brinkworth et al. (2013) observed G183−35 over a week in 2002 August and another week in 2003 May and found no evidence of variability or rotation on time-scales of less than a year. They concluded that this star is not varying at the 4 per cent peak-to-peak level on these time-scales. Fig. 4 shows time-series photometry of G183−35 obtained over two different nights in 2017 June. These data come from the 28–35 cm telescopes in Massachusetts and Oregon and slightly improve the limits on variability to a 3 $<A>$ detection limit of 15 mmag.

Fig. 5 shows the time-series photometry of the same target obtained at the McDonald Observatory 2.1 m telescope. The bottom panel shows the periodogram of all of the McDonald data combined. These data improve the limits on variability significantly, to a 4 $<A>$ limit of only 0.18 per cent. The periodogram for the combined data shows lots of aliasing, but the highest peak is at 151.2 μHz (period of 1.83 h) with an amplitude of 0.21 per cent. If we treat the June and July data separately, the highest peak shifts to 127.9 μHz with an amplitude 0.26 per cent and 174.1 μHz with an amplitude 0.22 per cent, respectively.

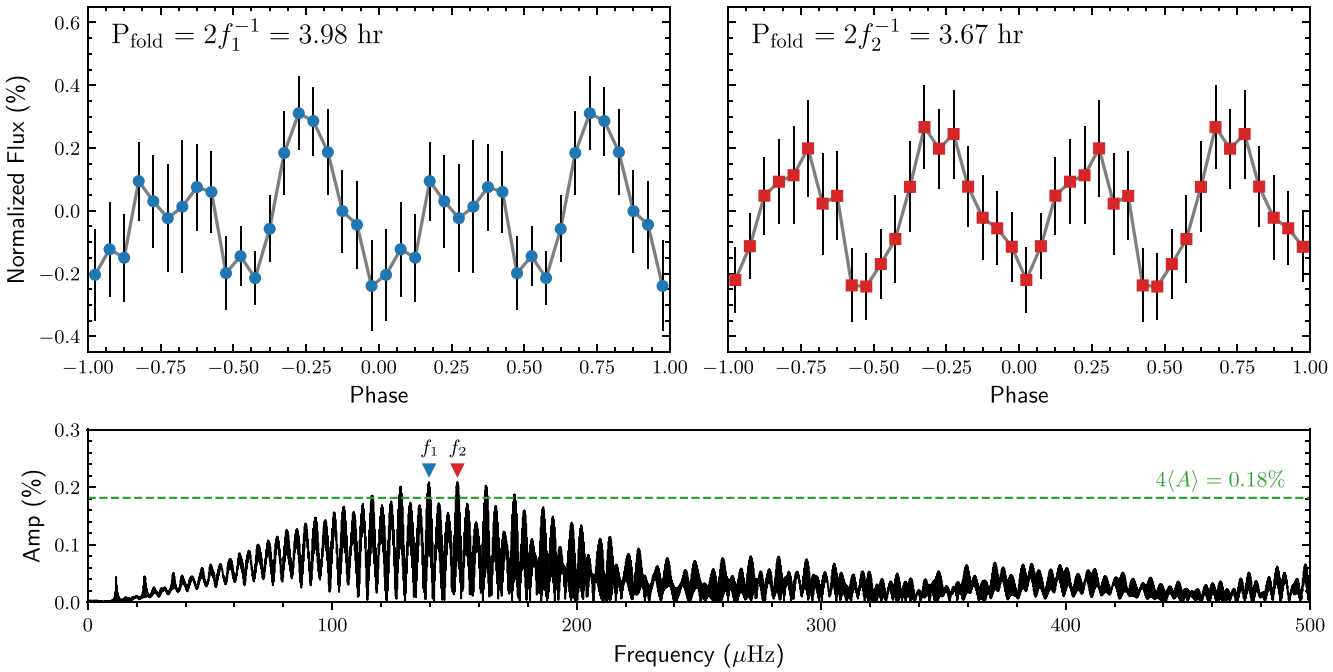

Figure 5. Time-series photometry of G183−35 obtained over 19.88 h at the McDonald Observatory 2.1 m telescope. The data are binned into 20 equally spaced bins per full phase, folded at 3.98 h (top left) and 3.67 h (top right). The bottom panel shows the periodogram for all of the McDonald data combined. The two highest peaks in the periodogram are labelled, and the dotted line shows the 4 <A> detection limit.

Considering that these frequencies are all offset from each other by integer multiples of the daily alias (11.57 μHz), these data sets are all consistent with the same frequency. The period that we get from the Gemini radial velocity data (3.98 h) has a half-period of 1.99 h and a corresponding frequency of 139.6 μHz. This is one daily alias away from the highest peak in both the June and the combined data, and three daily aliases away from the peak in the July data. Hence, even though the observed photometric variability is small, the detection is significant, and it matches the observed variability in the radial velocities of the central H α component, and also the changes in the equivalent width measurements of the inner and outer pairs of lines.

The top panels in Fig. 5 show the phase-folded McDonald light curve using the best-fit period from the spectroscopy (3.98 h) or photometry data (3.67 h). Both are acceptable due to the aliasing present, and both light curves show that G183−35 shows ≈0.4 per cent peak-to-peak variations over about 4 h.

4 DISCUSSION

4.1 Is this a binary system?

Leggett et al. (2018) used the U.S. Naval Observatory (USNO) parallaxes and photometry to derive $T_{\rm eff} = 6870 \pm 170$ K, $\log g = 8.07 \pm 0.06$, and $M = 0.63 \pm 0.05$ M$_\odot$ for G183−35 under the assumption of a single star. However, they also noted that there is a significant discrepancy between the USNO and Gaia Data Release 2 (Gaia Collaboration et al. 2018) parallax measurements for four of the stars in their sample, including G183−35. One of these stars (WD 0239+109) is a known double degenerate system, and Leggett et al. (2018) suggest that perhaps all four of these stars with discrepant USNO parallaxes are binary systems. Using the Gaia parallax, the best-fit parameters for G183−35 under the assumption of a single star change to $T_{\rm eff} = 6770 \pm 200$ K, $\log g = 8.28 \pm 0.05$, and $M = 0.77 \pm 0.04$ M$_\odot$.

A single magnetic DA white dwarf model with a temperature near 6800 K overpredicts the central component of the observed H α line profile in G183−35. To match the central component, the temperature needs to be reduced to about 5600 K, which is clearly inconsistent with the observed photometry. We note that there is another Gaia source (4578913734331945984) with $G = 19.89$ mag, $G_{\rm BP} - G_{\rm RP} = 1.33$ mag, and within 3.4 arcsec of G183−35. This other star is likely the source of the observed mid-infrared excess in the Wide-field Infrared Survey Explorer (WISE) photometry of this object (Leggett et al. 2018), but it is unlikely to affect the USNO parallax measurements.

Rolland & Bergeron (2015) performed a photometric and spectroscopic deconvolution of the suspected unresolved binaries in their sample by diluting their magnetic DAH white dwarf models with DC, DA, or DAH companions. They fit the temperatures and radii of both components and identified 8, 1, and 1 systems with likely DC, DA, and DAH white dwarf companions, respectively. They obtained temperatures of 5998 and 5849 K and $R_{\rm B}/R_{\rm A} = 1.128$ for the two magnetic white dwarf candidates in G183−35. These temperature and radii ratios along with the Gaia parallax imply a binary system containing a 0.97 M$_\odot$ primary and a 0.87 M$_\odot$ secondary.

If this is a double white dwarf system, and if the observed radial velocity variations of the central H α component (with semi-amplitude 33.5 km s^{-1}) are due to orbital motion, this implies a minimum mass companion of 0.09 M$_\odot$ for a 0.97 M$_\odot$ primary. Hence, if the velocity changes are due to orbital motion of a 0.97 + 0.87 M$_\odot$ binary, this would require a low-inclination ($i \approx 9°$) system. However, orbital motion in such a low inclination (almost face on) system cannot explain the inner and outer pairs of the H α components appearing and disappearing over several

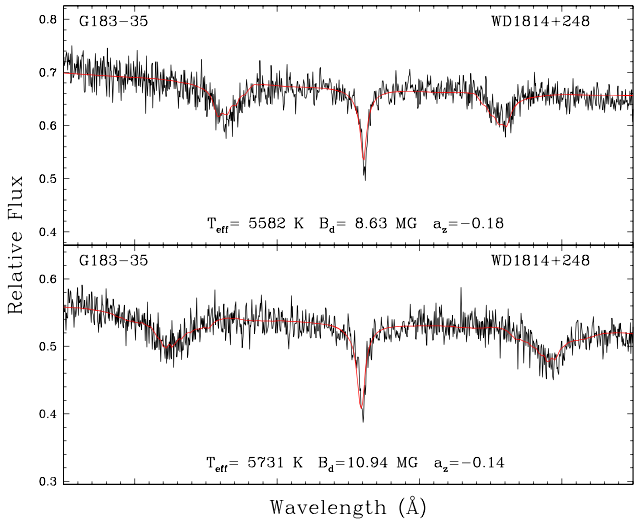

Figure 6. Our best fits (red lines) to two of the Gemini spectra using offset dipole models. We treat the effective temperature, the dipole strength B_d, and the offset a_z (in units of stellar radii) as free parameters. The top and bottom spectra show the inner and outer pairs of the split components, respectively.

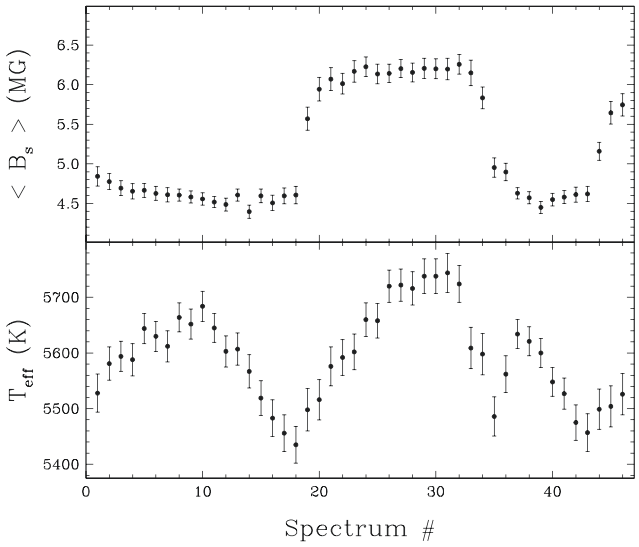

Figure 7. The average field strength over the visible stellar disc (top panel) and effective temperature (bottom panel) of the best-fit magnetic white dwarf model for each Gemini spectrum. Note that the first 32 spectra were obtained on the first night, the next 4 on the second night, and the last 10 were obtained on the last night of Gemini observations.

hours. An almost equal-mass binary would show significantly larger radial velocity shifts. For example, the $P = 1.154$ d binary NLTT 12758 consists of an $M = 0.69\,M_\odot$ magnetic white dwarf with an $M = 0.83\,M_\odot$ non-magnetic companion and displays up to 200 km s^{-1} radial velocity variations. Interestingly, NLTT 12758 shows photometric variations every 23 min due to the fast spinning magnetic white dwarf in that system. Hence, the observed spectroscopic variability in G183−35 is not due to orbital motion, but rather from changes in the line profiles due to the rotation of the magnetic white dwarf.

4.2 Rotational modulation

Photometric and spectroscopic variations due to rotation are commonly observed in magnetic white dwarfs. Photometric variability can be due to star spots or magnetic dichroism in high-field white dwarfs (Ferrario et al. 1997), whereas spectroscopic variability is usually caused by variations in the surface field strength that impacts the Zeeman-split components (Brinkworth et al. 2013).

To study the variability of the magnetic field structure on G183−35, we use offset dipole models to fit each Gemini spectrum under the assumption of a single magnetic DA white dwarf. The offset dipole models treat the dipole field strength B_d, viewing angle i, and the offset a_z (in units of stellar radii) as free parameters to reproduce the observed spectrum, and thus the magnetic field distribution across the stellar surface. Fig. 4 of Bergeron, Ruiz & Leggett (1992) illustrates the flexibility of the offset dipole models to match the field distribution across the stellar surface. In addition to B_d, i, and a_z, we also treat the effective temperature as a free parameter to get a reasonable fit to both the central Hα component and the inner/outer pair of lines. The viewing angle changes the asymmetry of the shifted components of the Hα line. We found that a viewing angle of $\sim$30° gives the best match to the data, and therefore we kept it constant in our fits.

Some of the Gemini spectra have both the inner and outer pairs of lines visible; we fit only the strongest pair of absorption features in those cases. Fig. 6 shows our model fits to two of the G183−35 spectra. The top spectrum shows the inner pair of lines, which indicate a dipole field strength of $B_d = 8.6$ MG, whereas the bottom spectrum shows the outer pair of lines, which indicate a field strength of $B_d = 10.9$ MG.

Fig. 7 shows the evolution of the mean field modulus (i.e. the average of the field strength over the visible stellar disk) and the best-fit temperature as a function of time. G183−35 switches between a low mean field modulus of ≈4.6 MG and a high mean field modulus of ≈6.2 MG over several hours. In addition, we find variations in the effective temperature of the best-fit model, which is a manifestation of the changes in the central Hα component. Of course, a time-dependent dipolar field strength is not realistic. Instead, the variations observed here are most likely due to rotation, with the magnetic axis offset with respect to the rotation axis, a model known as the oblique rotator (Stibbs 1950; Monaghan 1973). Because these two axes are not aligned, the observer sees a different magnetic field distribution across the stellar surface due to rotation.

There are several previously known examples of magnetic white dwarfs that display rapid evolution in their spectral line profiles. PG 1031+234 is one such system where Latter, Schmidt & Green (1987) observed significant changes in the spectrum of this object over the spin period of 3 h 24 min. They find two spectral features with field values ∼200 MG between rotational phases of 0.5 and 0.1, which then diffuse out and disappear at phase 0.15 as very high field zones appear with a field strength of 1000 MG and remain visible for phases of 0.15–0.5. Latter et al. (1987) conclude that their spectroscopic data are best explained by a field pattern with a slightly offset 500 MG global component with a localized magnetic spot with a central field of nearly 1000 MG.

EUVE J0317−85.5 is another rapidly changing system with a spin period of 12 min (Barstow et al. 1995). Vennes et al. (2003) display far-ultraviolet time-series spectroscopy of EUVE J0317−85.5 in their fig. 6. The spectra show the 1s0-2p-1 component of Lyα near 1300 Å between the phases of 0.3 and 0.7, but this line rapidly shifts to 1340 Å and remains at that wavelength between the phases 0.7 and 0.3. An overlap of high-field and low-field features is only apparent at phases 0.3 and 0.7. Vennes et al. (2003) conclude that a

high-field ($B \geq 425$ MG) magnetic spot with underlying lower field ($B \leq 185$ MG) surface would explain the variability in this system, including a rapid transition from low-field to high-field line spectra.

WD 1953−011 has a rotation period of 1.448 d, and its H α line profile is also best-explained by a two-component magnetic field that includes a weak (180–230 kG), large-scale component, and a strong (520 kG), localized component, i.e. a spot (Maxted et al. 2000; Valyavin et al. 2008). The large-scale component is almost always visible through the narrow splitting of the central H α line, and the spot is visible only at rotational phases of 0.25–0.7 through two broad features at 6554 and 6576 Å. Hence, the combined spectrum of WD 1953-011 would also display an H α line split into five components. Valyavin et al. (2008) find evidence for rotational variability of the projected effective size of the magnetic spot ranging from 0 to 12 per cent of the disc. Interestingly, the appearance/disappearance of the strong field component is very similar to the variability seen in G183−35. However, unlike in G183−35, the radial velocity of the central H α component in WD 1953-011 is constant to within a few km s^{-1} (Maxted et al. 2000). The similarities between the spectral evolution of G183−35 and the three other examples presented here strongly favour rotational modulation as the source of variability in G183−35.

4.3 Comparison with Ap/Bp stars

About 10 per cent of A and B type main-sequence stars host detectable magnetic fields. The majority of these stars are chemically peculiar, and therefore classified as Ap/Bp stars. These stars also show variations in their magnetic field strengths, spectral line profiles, and luminosities on time-scales related to their rotation periods (Bailey & Landstreet 2015, and references therein). Many of these stars show abundance variations over the stellar surface, which give rise to changes in their spectral line profiles. Analysing spectropolarimetry of three such stars, Kochukhov et al. (2017) and Kochukhov, Shultz & Neiner (2019) find distortions in the spectral line profiles of several metal lines that indicate large-scale, high-contrast abundance patterns over the stellar surface. They also detect significant changes in the magnetic field strength and topology, switching between a low-field and a high-field structure on the rotation period.

Bohlender, Rice & Hechler (2010) detected significant changes in the He line profiles of the Bp star a Centauri (HR 5378) and found that the He abundance geometry is consistent with a single spot model where one hemisphere of the star has an enhanced He abundance while the other hemisphere is He deficient. Similarly, Bailey et al. (2012) found H α line profile variations at different rotation phases in HD 133880. The line core shows excess absorption or emission compared to the average profile, which could be interpreted as radial velocity variations. Interestingly, the variations are only seen in the core of the H α line and they closely mimic the variations observed in Fe lines. Bailey et al. (2012) conclude that HD 133880 may be similar to a Centauri and it may also suffer from abundance anomalies between the different sides of the star.

Bailey, Grunhut & Landstreet (2015) report the detection of radial velocity variations of up to 35 km s^{-1} in the magnetic Ap star HD 94660. They emphasize that many Ap/Bp stars show variations due to shifts in the centre-of-gravity of the line profile due to the inhomogeneous surface distribution (e.g. spots), but these shifts are always smaller than the width of the line, and they also follow the rotation of the star. In the case of HD 94660 the rotation period is ≈2800 d, whereas the radial velocities vary with a ∼840 d period. Hence, the variations seen in this star is likely due to binarity.

Like most Ap/Bp stars, G183−35 shows variations in its magnetic field strength, spectral line profiles, and luminosity over a period of about 4 h. Hence, these variations are almost certainly due to the spin of the white dwarf. The distortions in the central H α component, which could be interpreted as radial velocity variations, can be explained by an inhomogeneous surface H distribution. He becomes invisible below about 11 000 K in white dwarf atmospheres. Hence, it is possible that G183−35 has a mixed H/He atmosphere with patchy H, and abundance variations across the stellar disk could lead to the observed distortions in the H α line.

It is intriguing that the majority of the magnetic DAs analysed by Rolland & Bergeron (2015) are all found in the same temperature range, between 5000 and 6000 K, in the so-called non-DA gap (Bergeron, Ruiz & Leggett 1997). It is also suspicious that the H α line profiles for the majority of these magnetic white dwarfs require dilution by a DC companion. There is a simpler explanation for the unusual line profiles; a chemically inhomogeneous mixed H/He atmosphere. Pereira, Bergeron & Wesemael (2005) found quasi-periodic variations in the strengths of the H and He lines over a period of ∼3.5 h in the DAB white dwarf GD 323. They found that a model with an inhomogeneous surface composition, resulting from the dilution of a thin hydrogen atmosphere with the underlying helium convection zone, best matches the observations. Hence, it is possible that G183−35 and the other unresolved binary candidates presented in Rolland & Bergeron (2015) have inhomogeneous surface composition with patchy H. Such a scenario would explain the observed variations in the line profiles and the discrepancy between the photometric and spectroscopic temperature measurements. In this scenario, only a fraction of the star would contribute to the H lines, and the temperature variations seen in Fig. 7 could be a manifestation of that. Follow-up observations of the other binary white dwarf candidates in Rolland & Bergeron (2015) can test this scenario.

5 CONCLUSIONS

We have presented time-series spectroscopy and photometry of the magnetic white dwarf G183−35. Even though the average spectrum shows an H α line split into five components, most spectra show only the inner or the outer pair of lines. The radial velocities of the central component, equivalent widths of the inner and outer pairs of lines, and the photometry all show variations on a period of ∼4 h. Orbital motion cannot explain the amplitude of the radial velocity variations and also the appearance and disappearance of the different sets of lines. On the other hand, rotation of a magnetic white dwarf with a chemically inhomogeneous surface, much like in Ap/Bp stars, can explain both spectroscopic and photometric variations seen in this star. Spectropolarimetry of G183−35 would help in understanding this object further by constraining its field topology.

ACKNOWLEDGEMENTS

We thank Jim Fuller for useful discussions and the referee, Stefano Bagnulo, for helpful suggestions. We gratefully acknowledge the support of the NSF under grant AST-1906379. This work is supported in part by the NSERC Canada and by the Fund FRQ-NT (Québec). Based on observations obtained at the Gemini Observatory, which is operated by the Association of Universities for Research in Astronomy, Inc., under a cooperative agreement with the NSF on behalf of the Gemini partnership: the National

Science Foundation (United States), National Research Council (Canada), CONICYT (Chile), Ministerio de Ciencia, Tecnología e Innovación Productiva (Argentina), Ministério da Ciência, Tecnologia e Inovação (Brazil), and Korea Astronomy and Space Science Institute (Republic of Korea).

REFERENCES

Bailey J. D., Landstreet J. D., 2015, A&A, 580, A81
Bailey J. D. et al., 2012, MNRAS, 423, 328
Bailey J. D., Grunhut J., Landstreet J. D., 2015, A&A, 575, A115
Barstow M. A., Jordan S., O'Donoghue D., Burleigh M. R., Napiwotzki R., Harrop-Allin M. K., 1995, MNRAS, 277, 971
Bergeron P., Ruiz M.-T., Leggett S. K., 1992, ApJ, 400, 315
Bergeron P., Ruiz M. T., Leggett S. K., 1997, ApJS, 108, 339
Bohlender D. A., Rice J. B., Hechler P., 2010, A&A, 520, A44
Briggs G. P., Ferrario L., Tout C. A., Wickramasinghe D. T., Hurley J. R., 2015, MNRAS, 447, 1713
Briggs G. P., Ferrario L., Tout C. A., Wickramasinghe D. T., 2018, MNRAS, 478, 899
Brinkworth C. S., Burleigh M. R., Lawrie K., Marsh T. R., Knigge C., 2013, ApJ, 773, 47
De Lee N. et al., 2013, AJ, 145, 155
Dobbie P. D., Baxter R., Külebi B., Parker Q. A., Koester D., Jordan S., Lodieu N., Euchner F., 2012, MNRAS, 421, 202
Ferrario L., Vennes S., Wickramasinghe D. T., Bailey J. A., Christian D. J., 1997, MNRAS, 292, 205
Ferrario L., de Martino D., Gänsicke B. T., 2015, Space Sci. Rev., 191, 111
Gaia Collaboration et al., 2018, A&A, 616, A10
Giclas H. L., Burnham R., Thomas N. G., 1971, Flagstaff. Lowell Observatory, Arizona
Girven J., Gänsicke B. T., Külebi B., Steeghs D., Jordan S., Marsh T. R., Koester D., 2010, MNRAS, 404, 159
Hintzen P., Strittmatter P. A., 1974, ApJ, 193, L111
Jordan S., Aznar Cuadrado R., Napiwotzki R., Schmid H. M., Solanki S. K., 2007, A&A, 462, 1097
Kawka A., Vennes S., Schmidt G. D., Wickramasinghe D. T., Koch R., 2007, ApJ, 654, 499
Kawka A., Briggs G. P., Vennes S., Ferrario L., Paunzen E., Wickramasinghe D. T., 2017, MNRAS, 466, 1127
Kochukhov O., Silvester J., Bailey J. D., Landstreet J. D., Wade G. A., 2017, A&A, 605, A13
Kochukhov O., Shultz M., Neiner C., 2019, A&A, 621, A47
Kurtz M. J., Mink D. J., 1998, PASP, 110, 934
Landstreet J. D., Bagnulo S., Valyavin G. G., Fossati L., Jordan S., Monin D., Wade G. A., 2012, A&A, 545, A30
Latter W. B., Schmidt G. D., Green R. F., 1987, ApJ, 320, 308
Leggett S. K. et al., 2018, ApJS, 239, 26
Liebert J., 1988, PASP, 100, 1302
Liebert J. et al., 2005, AJ, 129, 2376
Lomb N. R., 1976, Ap&SS, 39, 447
Maxted P. F. L., Ferrario L., Marsh T. R., Wickramasinghe D. T., 2000, MNRAS, 315, L41
Monaghan J. J., 1973, MNRAS, 163, 423
Pereira C., Bergeron P., Wesemael F., 2005, ApJ, 623, 1076
Putney A., 1995, ApJ, 451, L67
Rolland B., Bergeron P., 2015, in Dufour P., Bergeron P., Fontaine G., eds, ASP Conf. Ser. Vol. 493, 19th European Workshop on White Dwarfs. ASP, San Francisco, CA, p. 53
Scargle J. D., 1982, ApJ, 263, 835
Stibbs D. W. N., 1950, MNRAS, 110, 395
Tout C. A., Wickramasinghe D. T., Liebert J., Ferrario L., Pringle J. E., 2008, MNRAS, 387, 897
Valyavin G., Wade G. A., Bagnulo S., Szeifert T., Landstreet J. D., Han I., Burenkov A., 2008, ApJ, 683, 466
Vennes S., Schmidt G. D., Ferrario L., Christian D. J., Wickramasinghe D. T., Kawka A., 2003, ApJ, 593, 1040

This paper has been typeset from a TEX/LATEX file prepared by the author.